Inorganic Chemistry

Article

pubs.acs.org/IC

"Spider"-Shaped Porphyrins with Conjugated Pyridyl Anchoring Groups as Efficient Sensitizers for Dye-Sensitized Solar Cells

Christina Stangel,[†] Anthi Bagaki,[†] Panagiotis A. Angaridis,[‡] Georgios Charalambidis,[†] Ganesh D. Sharma,*[,§] and Athanasios G. Coutsolelos*[,†]

[†]Laboratory of Bioinorganic Chemistry, Department of Chemistry, University of Crete, Voutes Campus, 70013 Heraklion, Crete, Greece

[§]R&D Centre for Engineering and Science, JEC Group of Colleges, Jaipur Engineering College Campus, Kukas, Jaipur, Rajasthan 303101, India

[‡]Department of Chemistry, Aristotle University of Thessaloniki, Thessaloniki 54124, Greece

Supporting Information

ABSTRACT: Two novel "spider-shaped" porphyrins, *meso*-tetraaryl-substituted **1PV-Por** and zinc-metalated **1PV-Zn-Por**, bearing four oligo(*p*-phenylenevinylene) (oPPV) pyridyl groups with long dodecyloxy chains on the phenyl groups, have been synthesized. The presence of four pyridyl groups in both porphyrins, which allow them to act as anchoring groups upon coordination to various Lewis acid sites, the conjugated oPPV bridges, which offer the possibility of electronic communication between the porphyrin core and the pyridyl groups, and the dodecyloxy groups, which offer the advantage of high solubility in a variety of organic solvents of different polarities and could prevent porphyrin aggregation, renders porphyrins **1PV-Por** and **1PV-Zn-Por** very promising sensitizers for dye-sensitized solar cells (DSSCs). Photophysical measurements, together with electrochemistry experiments and density functional theory calculations, suggest that both porphyrins have frontier molecular orbital energy levels that favor electron injection and dye regeneration in DSSCs. Solar cells sensitized by **1PV-Por** and **1PV-Zn-Por** were fabricated, and it was found that they show power conversion efficiencies (PCEs) of 3.28 and 5.12%, respectively. Photovoltaic measurements ($J-V$ curves) together with incident photon-to-electron conversion efficiency spectra of the two cells reveal that the higher PCE value of the DSSC based on **1PV-Zn-Por** is ascribed to higher short-circuit current (J_{sc}), open-circuit voltage (V_{oc}), and dye loading values. Emission spectra and electrochemistry experiments suggest a greater driving force for injection of the photogenerated electrons into the TiO_2 conduction band for **1PV-Zn-Por** rather than its free-base analogue. Furthermore, electrochemical impedance spectroscopy measurements prove that the utilization of **1PV-Zn-Por** as a sensitizer offers a high charge recombination resistance and, therefore, leads to a longer electron lifetime.

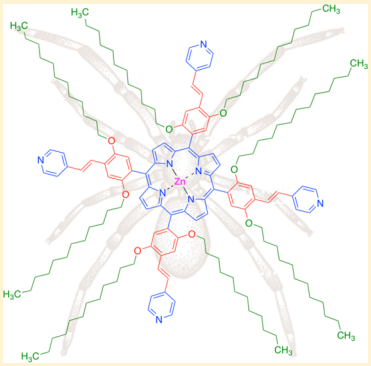

INTRODUCTION

Since the first report by O'Regan and Grätzel in 1991 for dye-sensitized solar cells (DSSCs),[1] intensive research efforts have been made toward the improvement of their photovoltaic efficiencies. Nowadays, DSSCs fabricated from environmentally friendly and inexpensive materials appear to be a very promising technology for low-cost and highly efficient solar energy conversion.[2−6] A typical device of this type consists of a wide-band-gap semiconductor photoanode (usually TiO_2) sensitized by a molecular dye, a redox electrolyte, and a platinum counter electrode. The sensitizer plays a key role in the operation of these devices because it is responsible for the absorption of solar radiation, the generation of excited electrons, and their injection into the TiO_2 conduction band (CB). Ruthenium complexes with polypyridyl ligands have been proven to be very efficient as DSSC sensitizers because they show intense and wide-range absorption from the visible to near-IR regions of the solar spectrum and result in DSSCs with power conversion efficiencies (PCEs) of 11%.[5,7,8] However, their practical application is hindered by their high cost and rarity and for environmental reasons. Porphyrins, because of their excellent light-harvesting potential in mimicking photosynthesis, stimulated significant interest as DSSC sensitizers.[9−11] Their photophysical characteristics, which include strong light absorptions in the visible region of the solar spectrum (with a strong Soret band around 420 nm and moderate Q bands in the 500−650 nm region), together with their thermal stability, make them ideal candidates for utilization as sensitizers in DSSCs.[12] Furthermore, porphyrins are versatile compounds because by functionalization of the meso and β-pyrrolic positions of the porphyrin ring, through rational molecular design and synthesis, their physicochemical properties can be appropriately tuned. Since then, Officer and co-workers reported in 2007 a DSSC sensitized by a porphyrin containing a conjugated side-chain anchoring group with a PCE

Received: April 10, 2014
Published: November 3, 2014

Scheme 1[a]

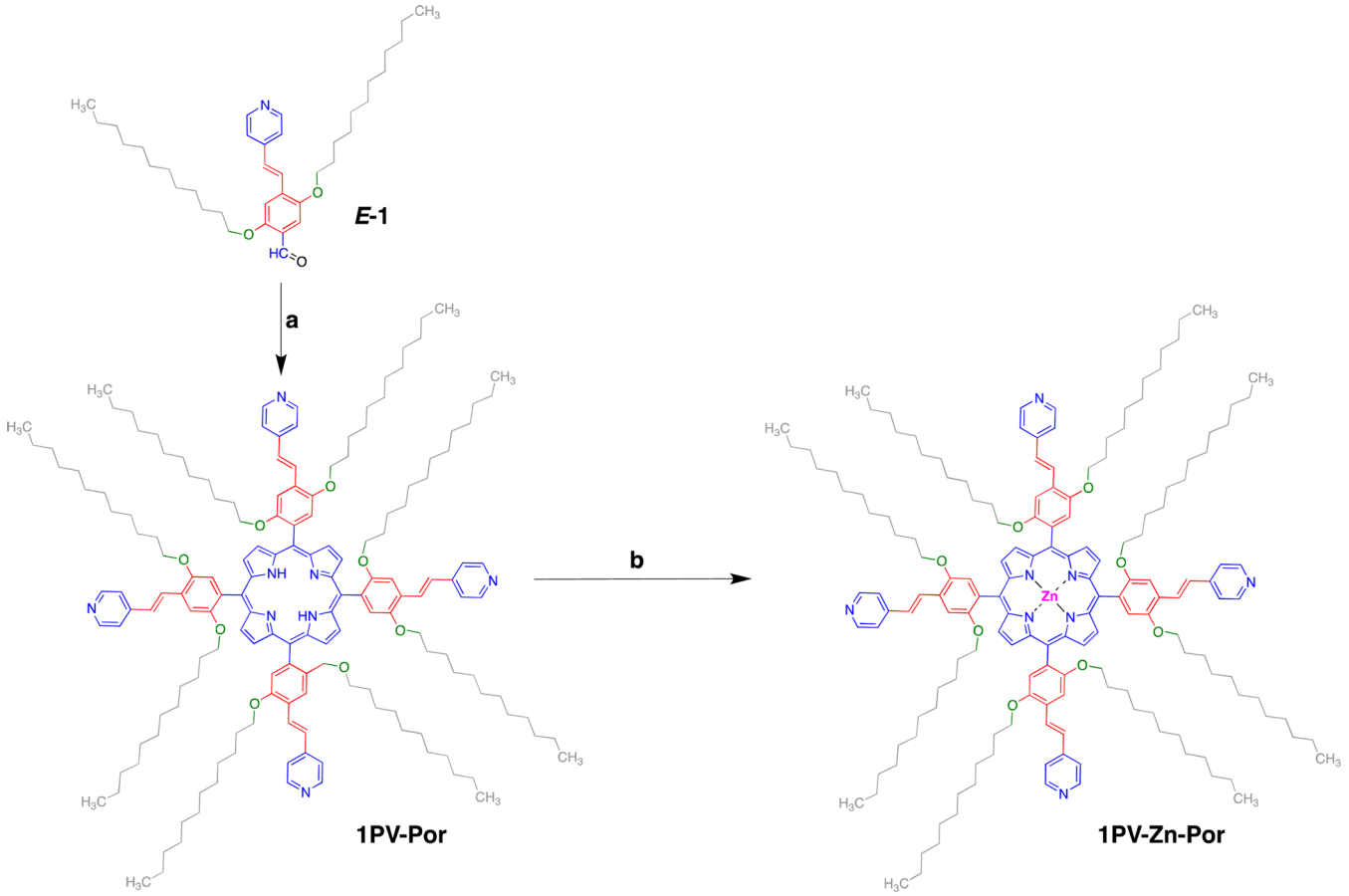

[a]Reagents and conditions: (a) pyrrole, propionic acid, 100 °C then reflux, 2 h; 6%; (b) $(CH_3COO)_2Zn{\cdot}2H_2O$, CH_2Cl_2/MeOH, rt, 95%.

value of 7.8%.[13] A few years later, Diau and co-workers reported porphyrin dyes with D−π−A architecture (D = donor, A = acceptor, and π = aromatic porphyrin ring), which yielded PCE values higher than 10%.[10,14,15] More recently, Diau, Grätzel, and co-workers further improved the efficiency of these types of porphyrin sensitizers above 12% by using a porphyrin with long alkoxy group substitutents, in combination with a cobalt-based electrolyte and an organic dye as the co-sensitizer.[16] However, the synthesis of this type of porphyrin dyes requires several complicated and time-consuming steps, preventing their commercial application.

To improve the efficiency of solar cells sensitized by porphyrins, one has to expand the light-harvesting ability of the porphyrin to the near-IR region. One way to achieve that is to covalently link a porphyrin macrocycle with other dyes or porphyrin units.[17−19] It has been shown that when two porphyrin molecules are linked through their meso positions either directly[20] or by suitable π-conjugated linkers,[21] strong electronic coupling between the porphyrins takes place, resulting in a splitting of their Soret bands and a broadening of their Q bands.[22] Indeed, porphyrin arrays linked through their meso positions by ethynyl groups exhibit broad spectral coverage and improved light-harvesting properties.[23] Recently, Grätzel and co-workers reported a new D−π−A type of porphyrin in which an electron acceptor group has been used as the linker between the benzoic acid anchoring group and the porphyrin macrocycle, resulting in a broadening of the porphyrin light absorption profile and leading to a PCE value of 13% using a Co^{2+}/Co^{3+}-containing electrolyte.[24,25]

In the majority of porphyrin sensitizers, as well as for most organic dye sensitizers, for attachment onto the TiO_2 surface of DSSCs, carboxylic acid groups have been widely used as electron-accepting anchoring groups. Except that they can be easily introduced into porphyrin derivatives through a variety of readily accessible precursors, they also offer very good electronic communication between the porphyrin unit and TiO_2 by forming a strong ester linkage with the TiO_2 surface, keeping the porphyrin macrocycle at an optimum orientation and distance from the TiO_2 surface and resulting in a fast and efficient electron injection.[26,27] Despite the remarkable performance of carboxylic acids in DSSCs, there is an ongoing quest for alternative anchoring groups for a number of different reasons, which include the positive shift (vs NHE) of the TiO_2 CB, which originates from H^+ intercalation into the TiO_2 surface during the dye-dipping process and lowers the open-circuit voltage (V_{oc}) of the DSSCs. Recently, new D−π−A organic dyes have been reported that utilize pyridyl units as electron-withdrawing anchoring groups.[28,29] Remarkably, these dyes, compared to the corresponding dyes with carboxyl acid anchoring groups, exhibit higher short-circuit photocurrent (J_{sc}) and PCE values. It seems that the coordinate bonds between the pyridyl groups of the dyes and the Lewis acid sites of the TiO_2 surface provide good electron communication between them and lead to very efficient electron injection. Recently, Wang and co-workers applied the same strategy for the

dx.doi.org/10.1021/ic502283d | Inorg. Chem. 2014, 53, 11871−11881

fabrication of DSSCs sensitized by D−π−A porphyrin sensitizers with pyridyl anchoring groups, which resulted in PCE values of ∼4.0%.[30]

Furthermore, recently, our research group reported the synthesis and utilization of simple porphyrin sensitizers with pyridyl anchoring groups directly attached to the porphyrin macrocycle for the fabrication of DSSCs, which reached a maximum PCE value of 3.9%.[31] In the present paper, we extended this approach by synthesizing new porphyrin sensitizers with pyridyl anchoring groups, in which the π-conjugated bridge oligo(*p*-phenylenevinylene) (oPPV) has been incorporated between the pyridyl units and the porphyrin core. More specifically, we present the synthesis and study of the DSSC performance of the "spider"-type porphyrins **1PV-Por** and **1PV-Zn-Por** (Scheme 1). The presence of the long alkoxy chains on the *meso*-phenyl groups offers the advantage of high solubility and prevents porphyrin aggregation, resulting in a PCE value of 5.12% for **1PV-Zn-Por**.

RESULTS AND DISCUSSION

Synthesis and Characterization. The syntheses of the two compounds are outlined in Scheme 1. **1PV-Por** was synthesized according to the Adler and Longo methodology, via the reaction of aldehyde (*E*)-2,5-Bis(dodecyloxy)-4-[2-(pyridin-4-yl)vinyl]benzaldehyde [(*E*)-**1**] with pyrrole in propionic acid under refluxing conditions, followed by chromatographic separation.[32] The synthesis of aldehyde (*E*)-**1** was achieved via a Wittig-type reaction.[33] It is well-known in porphyrin chemistry that the use of ortho-substituted aldehydes in condensation reactions with pyrrole leads to a mixture of four atropisomer meso-tetrasubstituted porphyrins, which usually have different polarities and can be separated chromatographically.[34−36] Similarly, in the present case, **1PV-Por** is obtained as a mixture of four atropisomers. In fact, from the ^{13}C NMR spectrum [see the Supporting Information (SI) for details], we can observe the different carbon peaks that correspond to the four atropisomers. However, their chromatographic separation has not been possible (at least in our hands). Apparently, the different orientations of the *o*-alkoxy substituents of the phenyl groups, because of their length, do not significantly differentiate the polarities of the atropisomers, making their separation nonfeasible. Metalation of the free-base porphyrin **1PV-Por** was carried out by the reaction with an excess of $(CH_3COO)_2Zn{\cdot}2H_2O$ in a mixture of CH_2Cl_2/methanol (MeOH) at room temperature for 24 h. After chromatographic purification, porphyrin **1PV-Zn-Por** was isolated in almost quantitative yield. The purity and identity of the two porphyrin dyes were confirmed by ^1H and ^{13}C NMR, UV−vis absorption, and matrix-assisted laser desorption ionization time-of-flight (MALDI-TOF) mass spectra and elemental analyses. Their ^1H NMR spectra confirm the *E* configuration of the double bonds by a coupling constant of approximately 16.5 Hz for the AB system, corresponding to the vinylic protons of the oPPV moiety in **1PV-Por**. Unfortunately, the ^1H NMR spectrum of **1PV-Zn-Por** showed only a few broad peaks, apparently because of strong intermolecular interactions in that concentration range (∼10^{-3} M), attributed to metal-to-ligand coordination between the zinc metal centers and pyridyl groups of different porphyrin units.[37] Furthermore, MALDI-TOF mass spectra showed the expected molecular ion peaks in every case: *m*/*z* 2500.8839 (**1PV-Por**); 2562.7975 (**1PV-Zn-Por**). Owing to the presence of the dodecyloxy groups, both porphyrins are highly soluble in a variety of organic solvents with different polarities like CH_2Cl_2, $CHCl_3$, tetrahydrofuran, and toluene.

The four terminal pyridyl groups of both porphyrins offer the ability of coordination to a variety of Lewis acids sites; therefore, porphyrins **1PV-Por** and **1PV-Zn-Por** have the potential to anchor to the TiO_2 surface of DSSC electrodes. Furthermore, the oPPV bridges between the porphyrin core and the terminal pyridyl groups offer the possibility of extended electronic communication between the porphyrin core and the TiO_2 surface of a photoanode. In addition, the presence of eight long dodecyloxy chains at the periphery of both porphyrins prevents the close proximity of different porphyrin units (through a combination of van der Waals, π−π-stacking, and charge-transfer interactions) and, therefore, diminishes the possibility of the formation of porphyrin aggregates on the TiO_2 surface, which is a major reason for the low performance of porphyrin-based DSSCs.

Photophysical Properties. The electronic absorption spectra of **1PV-Por** and **1PV-Zn-Por** in toluene solution are shown in Figure 1a,b (black lines). Both compounds show the characteristic absorption bands of porphyrin,[38] i.e., an intense Soret band in the 420−440 nm range and moderate Q bands between 510 and 650 nm. The absorption spectra of both

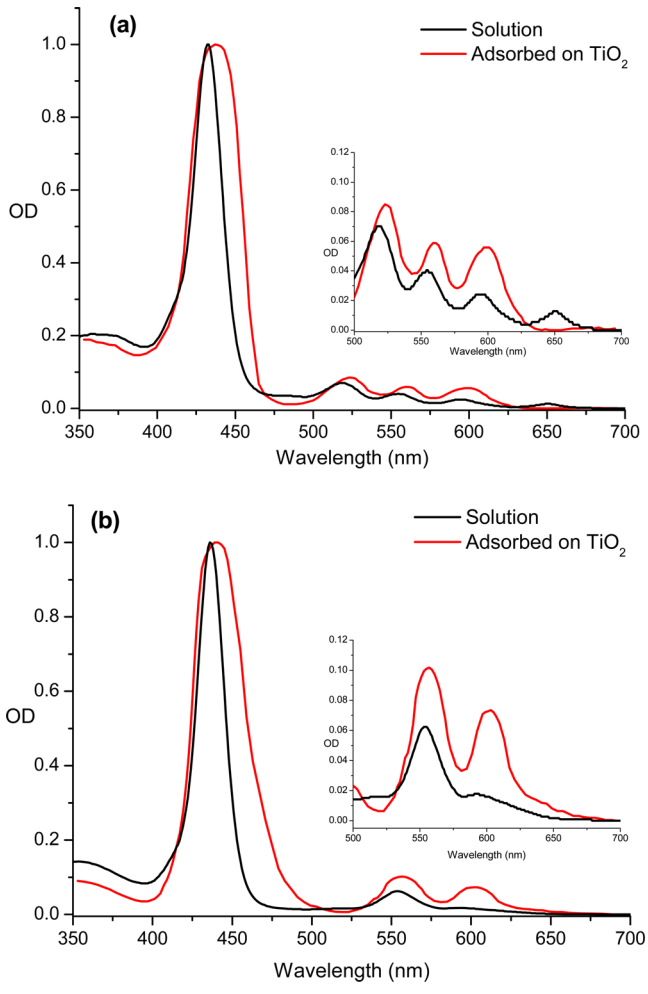

Figure 1. Normalized UV−vis absorption spectra of (a) **1PV-Por** and (b) **1PV-Zn-Por** in toluene solution (black lines) and after being adsorbed onto TiO_2 films (red lines). Insets: absorption spectra of **1PV-Por** and **1PV-Zn-Por** in the Q band region.

dx.doi.org/10.1021/ic502283d | *Inorg. Chem.* 2014, 53, 11871−11881

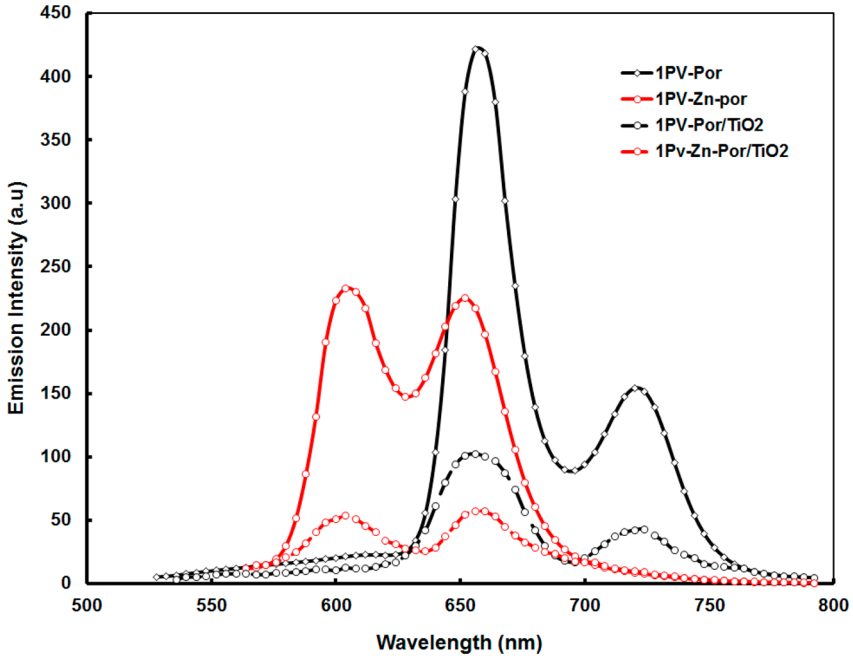

Figure 2. Room temperature emission spectra of **1PV-Por** (black lines) and **1PV-Zn-Por** (red lines) in toluene solution (solid lines) and after being adsorbed onto TiO_2 films (dashed lines), excited at Soret bands (432 nm for **1PV-Por** and 435 nm for **1PV-Zn-Por**).

porphyrins adsorbed onto TiO_2 films were also recorded (red lines in Figure 1a,b), in order to get information about their light-harvesting ability when they are part of solar cell photoanodes. Compared to the corresponding solution spectra, the absorption bands of both dyes anchored on the TiO_2 surface are broader and red-shifted. These observations are ascribed to interactions between the porphyrins and the TiO_2 surface. The optical band gaps of the two dyes **1PV-Por** and **1PV-Zn-Por** adsorbed onto thin TiO_2 films were estimated from their corresponding onset absorption edges and were calculated to be 1.94 and 1.88 eV, respectively.

The steady-state fluorescence (FL) spectra of **1PV-Por** and **1PV-Zn-Por** in toluene solution are shown in Figure 2 (black and red lines, respectively). Excitation of porphyrins at their Soret bands result in photoluminescence with two peaks of unequal intensities, i.e., 658 and 721 nm for **1PV-Por** and 605 and 652 nm for **1PV-Zn-Por**. The FL spectra of both dyes adsorbed onto the TiO_2 films excited at the same wavelength (Figure 2, dashed black and red line) were found to exhibit FL intensities that are significantly reduced. This FL quenching can be attributed to a photoinduced electron-transfer process from the porphyrin dyes to TiO_2.[39] The quenching is more pronounced in the **1PV-Zn-Por** dye than in the free-base porphyrin, indicating a more efficient photoinduced electron injection for the former, which leads to a greater photocurrent generation in the corresponding solar cell device.

Electrochemical Studies. For an effective sensitizer in a DSSC, efficient dye regeneration and electron injection processes require suitably aligned lowest unoccupied molecular orbital (LUMO) and highest occupied molecular orbital (HOMO) energy levels. The HOMO energy level of the dye should be lower than the corresponding redox potential of the electrolyte redox couple, while its LUMO energy level should be higher than the TiO_2 CB edge, enabling efficient dye regeneration and electron injection processes, respectively.[2,4,40,41]

The HOMO and LUMO energy levels of the porphyrin dyes were determined by square-wave voltammetry measurements (Figure 3), and they are summarized in Table 1. The LUMO energy levels of dyes **1PV-Por** and **1PV-Zn-Por**, estimated from the difference of the HOMO and optical band gap, were found to be −0.76 and −0.99 V vs NHE, respectively, which are higher than the TiO_2 CB (−0.5 V vs NHE). The corresponding HOMO energy levels were found to be 1.18 and 0.89 V vs NHE, respectively, and they are lower than the oxidation potential for the I_3^-/I^- redox couple. Therefore, there is a sufficient driving force for electron injection from the excited states of both porphyrins to the TiO_2 CB edge and for regeneration of the photooxidized dyes by transferring electrons from I_3^- of the electrolyte.

Density Functional Theory (DFT) Calculations. In order to gain insight into the molecular and electronic structures of porphyrins **1PV-Por** and **1PV-Zn-Por**, DFT calculations at the B3LYP/6-31G(*) level of theory were performed. Because of the fact that the total number of atoms of both compounds is too large for DFT calculations in our computer cluster, the molecules were simplified by replacing the long dodecyloxy groups at the 2 and 5 positions of the phenyl substituents of the porphyrin units with methoxy groups, which should not influence their HOMO and LUMO energy levels.

The gas-phase geometry-optimized structure of **1PV-Zn-Por** (the porphyrin with the better photovoltaic performance) is depicted in Figure 4, while the optimized coordinates are provided in Table S1 in the SI. The compound displays a planar central porphyrin scaffold, fulfilling the $p-\pi$ electron conjugation requirement, while the zinc atom lies on the same plane with the tetrapyrrole. The *meso*-aryl substituents of the porphyrin ring impose 4-fold rotation symmetry on the whole molecule, with the phenyl rings being in almost perpendicular orientation with respect to the porphyrin framework, with a twist angle of ∼80°. **1PV-Por** exhibits an almost identical gas-phase optimized structure.

dx.doi.org/10.1021/ic502283d | *Inorg. Chem.* 2014, 53, 11871−11881

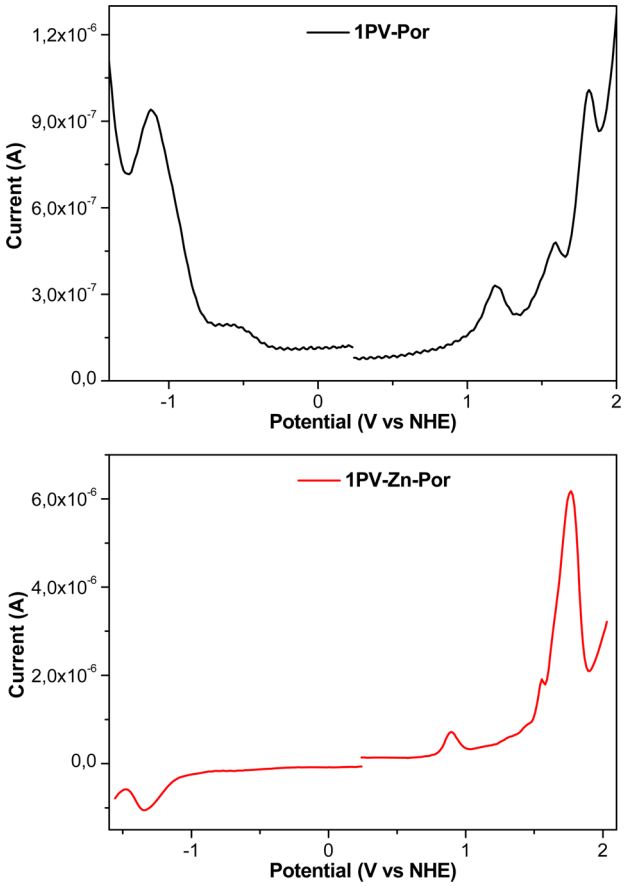

Figure 3. Square-wave voltammograms of porphyrins **1PV-Por** and **1PV-Zn-Por** in CH_2Cl_2. The redox couple wave for ferrocene/ferrocenium was observed at 0.65 V vs NHE.

Table 1. Oxidation and Reduction Potentials of Porphyrins 1PV-Por and 1PV-Zn-Por

compound	E_{ox1} (V vs NHE)	E_g^{opt} (eV)	E_{red1} (V vs NHE)	$E_{red} = E_{ox1} - E_g^{opt}$ (V vs NHE)	E_g^{elec}
1PV-Por	1.18	1.94	−1.08	−0.76	2.26
1PV-Zn-Por	0.89	1.88	−1.34	−0.99	2.23

The electron density distributions of the frontier and near-frontier molecular orbitals of **1PV-Zn-Por** are presented in Figure 5. Inspection of HOMO−1, HOMO, LUMO, and LUMO+1 reveals that they are mainly spread over the porphyrin unit and only partially delocalized over the phenyl rings of the meso substituents. No electron density was found on the conjugated bridge and pyridyl groups. In other words, these orbitals are essentially porphyrin-based π orbitals,[42] which are in quite good agreement with Gouterman's classic four-orbital model for porphyrins.[38] Nevertheless, HOMO−2, HOMO−3, LUMO+2, and LUMO+3 contain significant contributions from the meso substituent groups. Similar electron density distributions of the frontier molecular orbitals were also found for **1PV-Por**. These results suggest that neither of porphyrins do significantly promote intramolecular electron transfer, upon photoexcitation, to the pyridyl anchoring groups. This might be attributed to the long distance between the porphyrin unit and pyridyl anchoring groups.

The HOMO−LUMO gaps for **1PV-Por** and **1PV-Zn-Por** in CH_2Cl_2 solutions were calculated to be 2.737 and 2.800 eV, respectively, which are not significantly different from the HOMO−LUMO gaps estimated from square-wave voltammetry measurements.

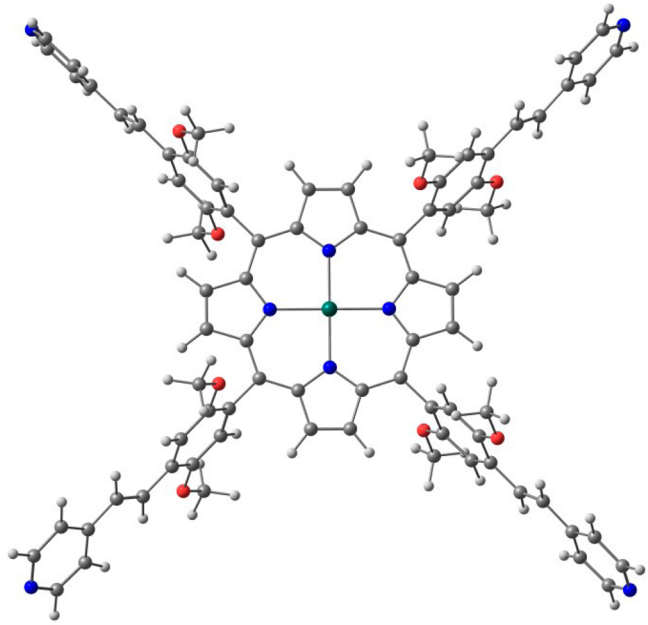

Figure 4. Gas-phase geometry-optimized structure of porphyrin **1PV-Zn-Por**. The gray, blue, white, red, and green balls represent the carbon, nitrogen, hydrogen, oxygen, and zinc atoms, respectively (dodecyloxy groups have been replaced by methoxy groups).

Photovoltaic Properties of DSSCs. The DSSCs sensitized by porphyrins **1PV-Por** and **1PV-Zn-Por** have been fabricated under identical conditions and studied. Their photovoltaic parameters are summarized in Table 2, and their corresponding current−voltage characteristics (J−V curves) are shown in Figure 6a. The DSSC sensitized by the free-base porphyrin **1PV-Por** exhibits J_{sc} = 8.86 mA/cm^2, V_{oc} = 0.64 V, and FF = 0.58, resulting in an overall PCE value of 3.28%. However, the solar cell sensitized by the zinc-metalated porphyrin **1PV-Zn-Por** displays enhanced photovoltaic parameters (J_{sc} = 11.25 mA/cm^2, V_{oc} = 0.68 V, and FF = 0.67), resulting in a higher PCE value of 5.12%.

The higher J_{sc} value of the **1PV-Zn-Por**-based solar cell is a major reason for its higher PCE value. Because J_{sc} of a solar cell depends on its incident photon-to-electron conversion efficiency (IPCE) response, the difference between the J_{sc} values of two solar cells should be reflected in their IPCE spectra. Indeed, as shown in Figure 6b, the IPCE response of the solar cell sensitized by **1PV-Zn-Por** is higher than the IPCE response of the solar cell sensitized by **1PV-Por**. In general, IPCE of a DSSC is the product of LHE, η_{inj}, and η_{cc} and can be expressed by the equation

$$\mathrm{IPCE}(\lambda) = \mathrm{LHE} \times \eta_{inj} \times \eta_{cc}$$

where LHE is the light-harvesting efficiency of the cell (which is related to the absorption profile of the sensitizing dye and the amount of dye adsorbed onto the TiO_2 surface), η_{inj} is the electron injection efficiency (which is related to the electron injection rate from the excited state of the sensitizer into the TiO_2 CB), and η_{cc} is the charge collection efficiency (which is related to the recombination rate of injected electrons with the oxidized dye or redox couple in the electrolyte).

dx.doi.org/10.1021/ic502283d | Inorg. Chem. 2014, 53, 11871−11881

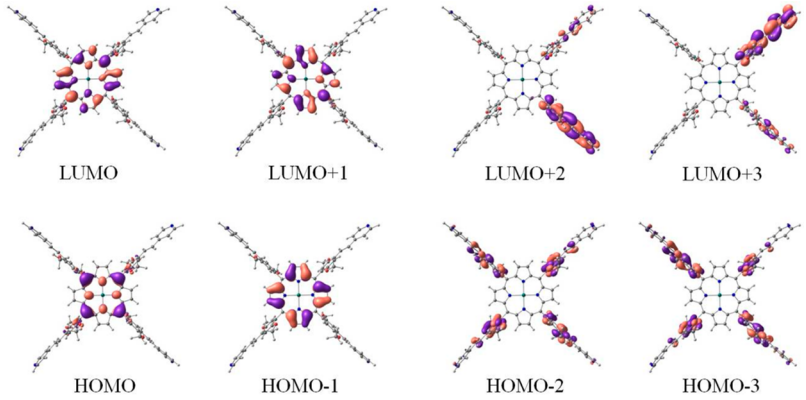

Figure 5. Frontier and near-frontier molecular orbitals of porphyrin **1PV-Zn-Por**.

Table 2. Photovoltaic Parameters of DSSCs Based on 1PV-Por and 1PV-Zn-Por

DSSC	J_{sc} (mA/cm^2)	V_{oc} (V)	FF	PCE (%)
sensitized by **1PV-Por**	8.86	0.64	0.58	3.28
sensitized by **1PV-Zn-Por**	11.25	0.68	0.67	5.12

Among the three factors that affect IPCE, LHE plays a very important role. The **1PV-Zn-Por**-based DSSC exhibits a higher LHE value than **1PV-Por** (Figure 7). Because both dyes display very similar absorption profiles, the main factor that determines the higher LHE value of the **1PV-Zn-Por**-based solar cell is the higher amount of dye adsorbed (or dye loading) onto the TiO_2 surface. In order to estimate the dye loading values of the two solar cells, the dye-sensitized TiO_2 electrodes were immersed in a mixture of CH_2Cl_2 and NaOH(aq) solution, and the absorption spectra of desorbed dye solutions were measured. The dye loading values were found to be 2.68×10^{-7} and 3.14×10^{-7} mol/cm^2 for the **1PV-Por**- and **1PV-Zn-Por**-based solar cells, respectively. The higher dye loading value of the **1PV-Zn-Por**-based DSSC may be attributed to the more effective binding of this porphyrin onto the TiO_2 surface. This may be rationalized by resonance conjugation between the zinc metal center and pyridyl anchoring groups, which increases the basicity of **1PV-Zn-Por** and, therefore, its affinity for TiO_2. As shown in the FL spectra of the dye adsorbed onto the TiO_2 film, the FL quenching is more for **1PV-Zn-Por**/TiO_2 than for **1PV-Por**/TiO_2, which also indicates that the long-range charge separation in the former is higher than that in the latter, resulting in a higher value of IPCE. In addition, as can be concluded from the electrochemical data of the dyes, as shown in Table 1, the driving force for electron injection from the photoexcited dye is higher for porphyrin **1PV-Zn-Por** (0.73 V vs NHE) than for free porphyrin (0.5 V vs NHE), which suggests a more efficient electron injection for the **1PV-Zn-Por**-based DSSC. In total, the combined effect of the higher LHE and η_{inj} values for the **1PV-Zn-Por**-based DSSC leads to an improved IPCE response and enhanced J_{sc} value and, therefore, to a higher overall PCE value. These results are in agreement with the observation of other scientists that zinc-metalated porphyrins have a greater driving force for injection of the photogenerated electrons into the TiO_2 CB than their free-base analogues (which can be attributed to the higher singlet excited states of the former), resulting in faster electron injection dynamics and better photovoltaic responses.[43]

The enhanced photovoltaic performance of the **1PV-Zn-Por**-based solar cell is also related to its enhanced V_{oc} value. The V_{oc} value of a TiO_2-based DSSC is a measure of the potential difference between the Fermi level of TiO_2 (E_F) and the redox potential (E_{redox}) of the redox couple in the electrolyte. V_{oc} and E_F can be expressed according to the relationships[44]

$$V_{oc} = E_{redox} - E_F$$

$$E_F = E_{CB} + kT \ln\left(\frac{n_c}{N_c}\right)$$

where k is the Boltzmann constant, T is the temperature, n_c is the free electron density, and N_c is the density of the accessible states in the CB. Because both DSSCs are based on the same redox couple, they have the same E_{redox} value; hence, their V_{oc} values entirely depend on the corresponding E_{CB} and n_c values. E_{CB} is determined by the surface charge of TiO_2, while n_c is determined by the balance between electron injection and electron recombination. Different dyes affect the position of the TiO_2 CB edge differently because any change in the surface charge will shift the position of the TiO_2 CB edge.[45] Therefore, because the electron injection process is more efficient for the DSSC based on **1PV-Zn-Por**, the cell exhibits a higher n_c value, which leads to a higher V_{oc} value.

Electrochemical impedance spectroscopy (EIS) has been a very powerful tool in the understanding of interfacial charge-transfer processes in DSSCs.[46−48] To clarify the relationship between the charge-transfer processes and photovoltaic properties in the DSSCs, EIS spectra of the two solar cells in dark conditions were recorded, using an applied direct-current bias of −0.65 V. The typical Nyquist plots of EIS of the two solar cell devices are shown in Figure 8a. The high-frequency semicircle in the left side of the spectrum is associated with the charge-transfer resistance at the platinum counter electrode/electrolyte interface, while the semicircle in the middle-frequency range corresponds to the charge recombination resistance at the TiO_2/dye/electrolyte interface. The radii of both semicircles are larger for the **1PV-Zn-Por**-based solar cell than for the **1PV-Por**-based solar cell, which indicates a higher charge-transfer resistance at the interface. These results are further supported by measuring the $J-V$ characteristics of the two DSSCs in the dark (Figure 9). The dark current is a measure of the recombination process in a DSSC. Because the dark current of the **1PV-Zn-Por**-based DSSC is lower than that of the **1PV-Por**-based DSSC, the former device exhibits a higher charge recombination resistance at the TiO_2/dye/electrolyte interface.

dx.doi.org/10.1021/ic502283d | *Inorg. Chem.* 2014, 53, 11871−11881

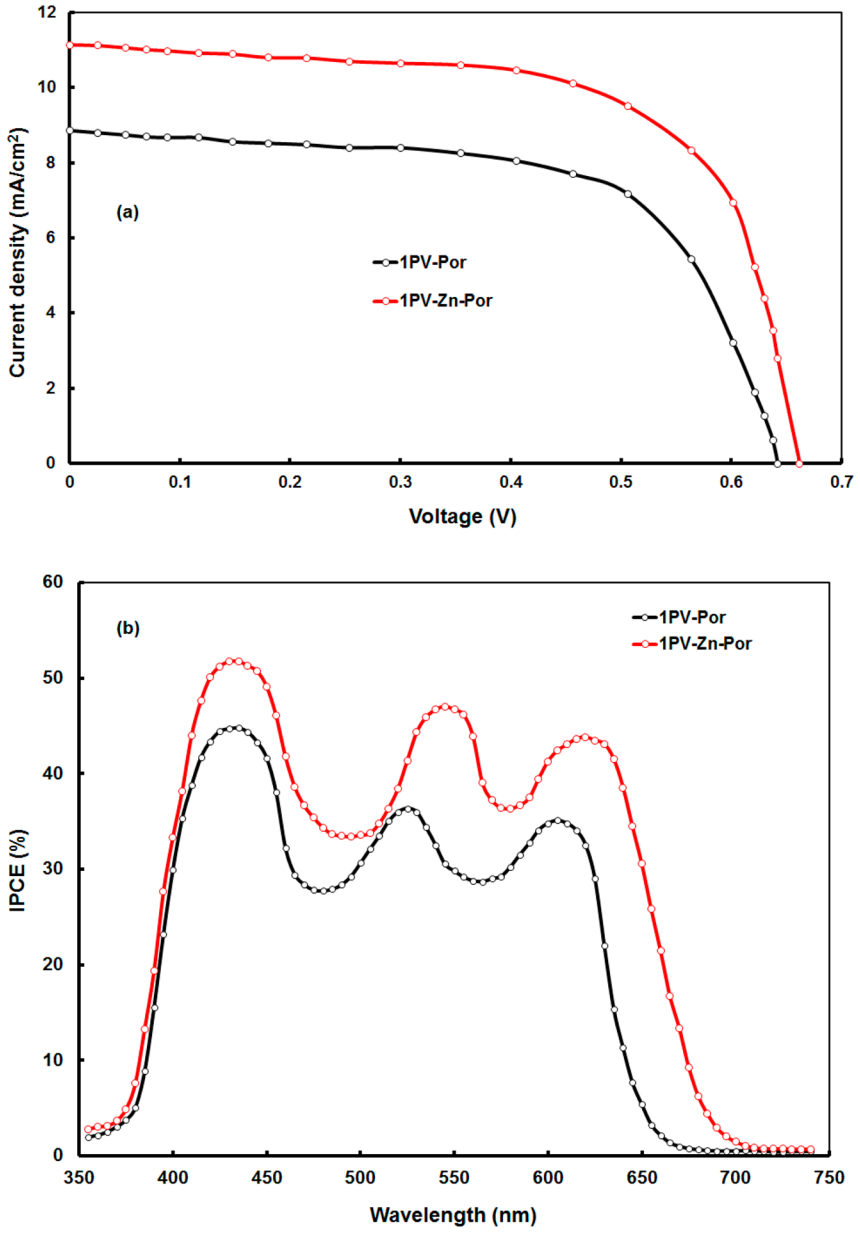

Figure 6. (a) J–V characteristics under illumination and (b) IPCE spectra of DSSCs sensitized by porphyrins **1PV-Por** (black lines) and **1PV-Zn-Por** (red lines).

The Bode phase plots of EIS spectra of the two devices are shown in Figure 8b. The peak in the high-frequency region corresponds to the charge-transfer rate at the counter electrode, while the peaks in the intermediate-frequency region in these plots correspond to the TiO_2/dye/electrolyte interface, which are related to the charge recombination rates of the solar cells and the corresponding electron lifetimes. A higher-frequency peak is indicative of a shorter electron lifetime. The electron lifetimes (τ_e) for the DSSC devices were calculated according to the relationship

$$\tau_e = \frac{1}{2\pi f_{max}}$$

where f_{max} is the frequency at the maxima of the middle-frequency semicircles in Bode phase plots, which were found to be 21 and 29 ms, 1PV-Por and 1PV-Zn-Por, respectively. The longer electron lifetime for the **1PV-Zn-Por**-based DSSC demonstrates a slower charge recombination process, which may result in a higher V_{oc} value. This may be ascribed to a more effective suppression of charge recombination between the injected electron and electrolyte because of the formation of a more compact hydrophobic layer at the TiO_2 surface and retardation of the diffusion of I_3^- into the nanoporous TiO_2 electrode.

V_{oc} also depends on the recombination reaction rate of the injected electron with I_3^- of the electrolyte, as indicated by the relationship

$$V_{oc} = \frac{kT}{q} \ln\left(\frac{\eta\phi_0}{n_0 k_{et}[I_3^-]}\right)$$

where η is the quantum yield of the photogenerated electrons for a given photon flux ϕ_0, n_0 is the electron density on the CB in the dark, and k_{et} reflects the recombination reaction rate of the injected electrons with I_3^- of the electrolyte. As evidenced

dx.doi.org/10.1021/ic502283d | Inorg. Chem. 2014, 53, 11871−11881

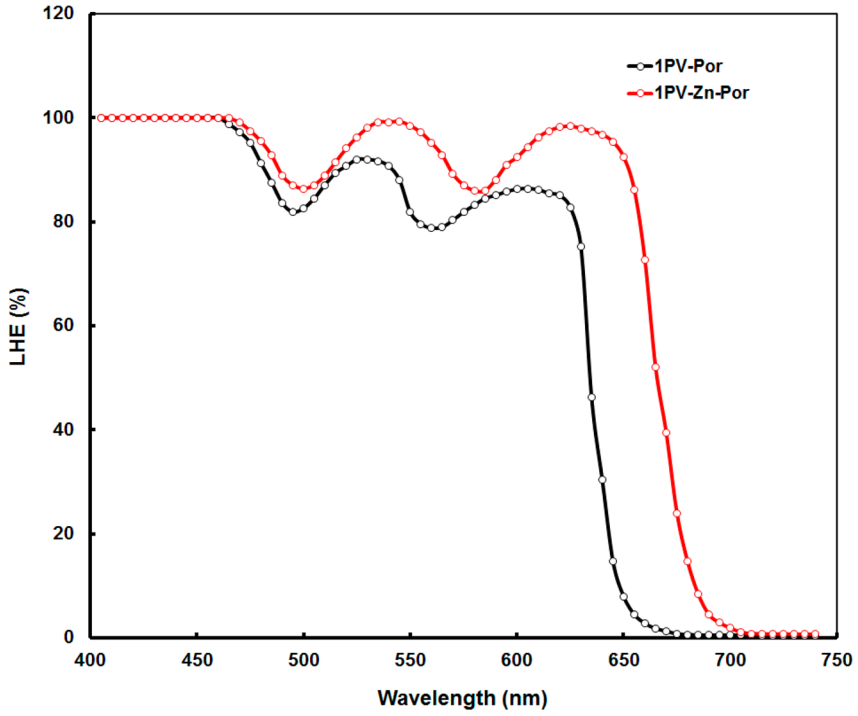

Figure 7. LHEs of **1PV-Por**- and **1PV-Zn-Por**-coated TiO_2 films.

from the lower dark current of porphyrin **1PV-Zn-Por** and the longer electron lifetime for the DSSC based on **1PV-Zn-Por**, the above processes lead to the higher value of V_{oc} for this device.

EXPERIMENTAL SECTION

^1H and ^{13}C NMR spectra were recorded on Bruker AMX-500 MHz and Bruker DPX-300 MHz spectrometers as solutions in deuterated solvents by using the solvent peak as the internal standard. High-resolution mass spectrometry spectra were recorded on a Bruker ultrafleXtreme MALDI-TOF/TOF spectrometer, using *trans*-2-[3-(4-*tert*-butylphenyl)-2-methyl-2-propenylidene]malononitrile as the matrix. Elemental analyses were performed with a Perkin-Elmer 240B elemental analyzer.

Photophysical Measurements. A Shimadzu UV-1700 spectrophotometer was used for the UV−vis absorption spectra measurements, and the emission spectra were measured on a JASCO FP-6500 fluorescence spectrophotometer.

Electrochemistry. An AutoLab PGSTAT20 potentiostat was used for square-wave voltammetry experiments, which were carried out at room temperature. Measurements were carried out in freshly distilled and deoxygenated CH_2Cl_2, at a rate of 100 mV/s, with a solute concentration of ∼1.0 mM in the presence of tetrabutylammonium tetrafluoroborate (0.1 M) as the supporting electrolyte. A three-electrode cell setup was used with a platinum working electrode, a saturated calomel (SCE) reference electrode, and a platinum wire counter electrode.

Computational Details. All of the appropriate details used for the computational measurements have been reported elsewhere.[49,50]

Fabrication and Characterization of DSSCs. A detailed description of the preparation of the electrodes was published by our group elsewhere.[51,52] The *J*−*V* characteristics of the DSSCs were measured using a computer-controlled Keithley sourcemeter, under standard air mass (AM 1.5, 100 mW/cm^2), using a xenon lamp coupled with an optical filter. The IPCE spectra of the DSSCs were recorded using a system consisting of a monochromator and a xenon lamp, and the photocurrent in short-circuit conditions was measured using a Keithley electrometer. The EIS measurements of DSSCs, in the dark, were carried out by applying a bias equivalent to the open-circuit voltage, i.e. −0.65 V, and recording over a frequency of 0.1−100 kHz with an alternating-current amplitude of 10 mV. The above measurements were carried out using a CHN electrochemical workstation equipped with *FRA* software to analyze the data.

Materials and Techniques. Reagents and solvents were purchased as reagent grade from the usual commercial sources and used without further purification, unless otherwise stated. (*E*)-2,5-Bis(dodecyloxy)-4-[2-(pyridin-4-yl)vinyl]benzaldehyde [(*E*)-**1**] was previously synthesized from our group.[53] Thin-layer chromatography was performed on silica gel 60 F_{254} plates, while chromatographic separations were carried out using silica gel 60, SDS, 70−230 mesh ASTM.

1PV-Por. A solution of (*E*)-**1** (0.200 g, 0.346 mmol) in propionic acid (10 mL) was heated to 100 °C, and pyrrole (0.024 mL, 0.346 mmol) was added dropwise. The reaction mixture was heated under reflux for 2 h, and the resulting solution was evaporated to dryness under vacuum. The crude residue was purified by column chromatography (SiO_2; CH_2Cl_2/MeOH, 100:3) to obtain the four-atropisomer mixture of **1PV-Por** as a red-purple solid (0.052 g, 6% yield). This purification of the product was repeated two more times. ^1H NMR (500 MHz, $CDCl_3$): δ −2.62 (s, 2H), 0.54 (m, 8H), 0.85 (m, 24H), 1.17 (m, 136H), 1.51 (m, 8H), 1.89 (m, 8H), 3.86 (m, 8H), 4.06 (m, 8H), 7.38 (d, J = 16.5 Hz, 4H), 7.55 (m, 12H), 7.62 (m, 4H), 8.00 (d, J = 16.5 Hz, 4H), 8.67 (m, 8H), 8.86 (s, 8H). ^{13}C NMR (125 MHz, $CDCl_3$): δ 14.20, 14.22, 14.25, 22.79, 22.82, 25.30, 25.34, 25.40, 26.43, 26.45, 26.48, 28.73, 28.77, 28.85, 28.90, 28.96, 29.01, 29.10, 29.16, 29.21, 29.29, 29.32, 29.34, 29.37, 29.40, 29.45, 29.50, 29.57, 29.59, 29.61, 29.68, 29.74, 29.76, 29.79, 31.90, 31.95, 32.01, 69.64, 69.74, 69.82, 111.22, 111.30, 111.44, 111.55, 115.50, 115.53, 115.59, 115.69, 120.97, 121.07, 121.14, 126.09, 126.13, 126.80, 128.72, 128.75, 128.94, 131.00, 133.35, 133.44, 133.60, 133.65, 145.72, 150.20, 153.45. UV−vis [toluene; λ_{max}, nm (ε, mM^{-1} cm^{-1})]: 300 (44.7), 363 (43.4), 432 (220.5), 518 (13.9), 554 (7.4), 594 (3.7), 651 (1.2). HRMS (MALDI-TOF). Calcd for $C_{168}H_{243}N_8O_8$: m/z 2500.8854 ([M + H]$^+$). Found: m/z 2500.8839. Anal. Calcd for $C_{168}H_{242}N_8O_8$: C, 80.65; H, 9.75; N, 4.48. Found: C, 80.51; H, 9.88; N, 4.30.

1PV-Zn-Por. Porphyrin **1PV-Por** (0.020 g, 0.008 mmol) was dissolved in a 10 mL mixture of CH_2Cl_2/MeOH (3:1 in volume ratio), and $(CH_3COO)_2Zn{\cdot}2H_2O$ (0.026 g, 0.120 mmol) was added. The reaction mixture was stirred at room temperature for 24 h. After the

dx.doi.org/10.1021/ic502283d | *Inorg. Chem.* 2014, 53, 11871−11881

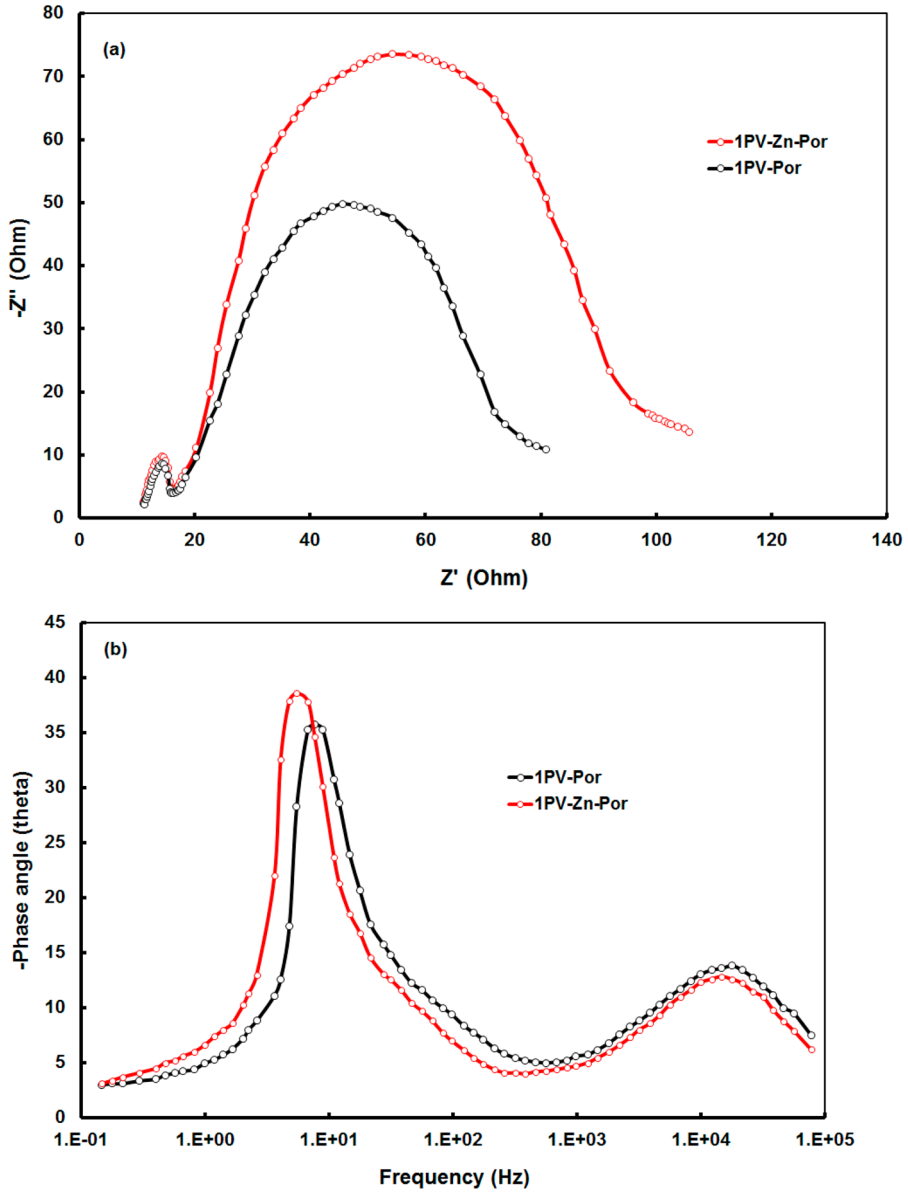

Figure 8. (a) Nyquist plots and (b) Bode phase plots of EIS spectra in the dark of DSSCs based on porphyrins **1PV-Por** (black lines) and **1PV-Zn-Por** (red lines).

volatiles were distilled off under vacuum, the resulting residue was transferred to the top of a short silica gel column and eluted with CH_2Cl_2/MeOH (100:3) to collect the desired product **1PV-Zn-Por** as a purple solid (0.019 g, 95%). The ^{1}H NMR spectrum of **1PV-Zn-Por** showed broad peaks probably because of the development of strong intramolecular interactions, in the particular concentration range between the pyridyl groups and zinc metal centers of neighboring porphyrin units. ^{13}C NMR (125 MHz, $CDCl_3$): δ 14.19, 14.22, 22.77, 25.24, 26.38, 28.92, 29.45, 29.75, 32.00, 69.55, 111.58, 115.65, 120.91, 125.36, 125.26, 128.96, 129.47, 131.23, 135.24, 135.43, 145.74, 150.12, 153.63. UV−vis [toluene; λ_{max}, nm (ε, mM^{-1} cm^{-1})]: 304 (55.6), 356 (40.6), 435 (260.4), 553 (17.6), 593 (5.3) nm. HRMS (MALDI-TOF). Calcd for $C_{168}H_{241}N_8O_8Zn$: m/z 2562.7989 ([M + H]$^+$). Found: m/z 2562.7975. Anal. Calcd for $C_{168}H_{240}N_8O_8Zn$: C, 78.66; H, 9.43; N, 4.37. Found: C, 78.79; H, 9.31; N, 4.25.

CONCLUSIONS

We report herein the synthesis and characterization of two *meso*-tetraaryl-substituted "spider-shaped" porphyrins, i.e., free-base **1PV-Por** and zinc-metalated **1PV-Zn-Por** bearing oligophenylenevinylene moieties, long dodecyloxy chains, and pyridyl groups, as well as their use as sensitizers for the fabrication DSSCs. Both porphyrins contain terminal pyridyl groups, which can act as anchoring groups for the attachment of porphyrins onto the TiO_2 surface of DSSC photoanodes, conjugated oPPV bridges, which offer the possibility of electronic communication between the porphyrin core and terminal pyridyl groups, as well as long aliphatic groups, which can prevent porphyrin aggregation on the TiO_2 surface. Photophysical and square-wave voltammetry measurements of both dyes, together with DFT calculations, revealed suitable HOMO and LUMO energy levels for their use as sensitizers in DSSCs. DSSCs based on porphyrins **1PV-Por** and **1PV-Zn-Por** were fabricated, revealing efficient sensitization, and PCE values of 3.28 and 5.12%, respectively. The higher PCE value of the latter is attributed to its higher photovoltaic parameters and larger dye loading. This is probably due to a faster electron injection process for the solar cell based on porphyrin **1PV-Zn-Por**, as suggested by emission spectra and electrochemistry

dx.doi.org/10.1021/ic502283d | *Inorg. Chem.* 2014, 53, 11871−11881

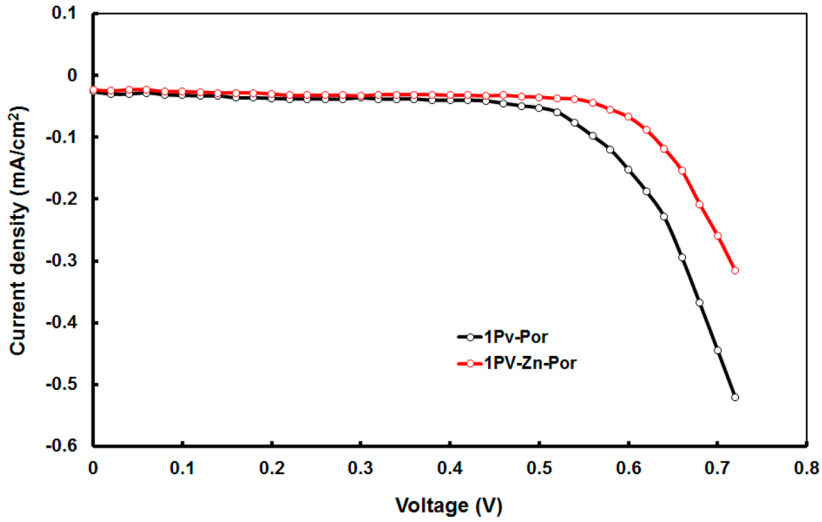

Figure 9. *J*–*V* characteristics of the DSSCs sensitized by porphyrins **1PV-Por** (black line) and **1PV-Zn-Por** (red line) in the dark.

measurements of both porphyrins. Furthermore, EIS measurements revealed a longer electron lifetime and higher charge recombination resistance for the **1PV-Zn-Por**-based solar cell.

■ ASSOCIATED CONTENT

Supporting Information

^{1}H and ^{13}C NMR spectra of **1PV-Por** and **1PV-Zn-Por** and coordinates of gas-phase geometry-optimized structure of **1PV-Zn-Por** as calculated by DFT calculations. This material is available free of charge via the Internet at http://pubs.acs.org.

■ AUTHOR INFORMATION

Corresponding Authors

*E-mail: gdsharma273@gmail.com.
*E-mail: coutsole@chemistry.uoc.gr.

Notes

The authors declare no competing financial interest.

■ ACKNOWLEDGMENTS

This research has been financed by the European Commission (FP7-REGPOT-2008-1, Project BIOSOLENUTI No. 229927), which is greatly acknowledged. Also this research has been cofinanced by the European Union (European Social Fund) and Greek national funds through the Operational Program "Education and Lifelong Learning" of the National Strategic Reference Framework, Research Funding Program: Heraklitos II and THALIS-UOA-MIS 377252. Finally, a special research account of the University of Crete is also acknowledged.

■ REFERENCES

(1) O'Regan, B.; Gratzel, M. *Nature* **1991**, *353*, 737.
(2) Hagfeldt, A.; Boschloo, G.; Sun, L.; Kloo, L.; Pettersson, H. *Chem. Rev.* **2010**, *110*, 6595.
(3) Peter, L. M. *J. Phys. Chem. Lett.* **2011**, *2*, 1861.
(4) Zhang, S. F.; Yang, X. D.; Numata, Y. H.; Han, L. Y. *Energy Environ. Sci.* **2013**, *6*, 1443.
(5) Grätzel, M. *Acc. Chem. Res.* **2009**, *42*, 1788.
(6) Han, L.; Islam, A.; Chen, H.; Malapaka, C.; Chiranjeevi, B.; Zhang, S.; Yang, X.; Yanagida, M. *Energy Environ. Sci.* **2012**, *5*, 6057.
(7) Cao, Y.; Bai, Y.; Yu, Q.; Cheng, Y.; Liu, S.; Shi, D.; Gao, F.; Wang, P. *J. Phys. Chem. C* **2009**, *113*, 6290.
(8) Yu, Q.; Wang, Y.; Yi, Z.; Zu, N.; Zhang, J.; Zhang, M.; Wang, P. *ACS Nano* **2010**, *4*, 6032.
(9) Lan, C.-M.; Wu, H.-P.; Pan, T.-Y.; Chang, C.-W.; Chao, W.-S.; Chen, C.-T.; Wang, C.-L.; Lin, C.-Y.; Diau, E. W.-G. *Energy Environ. Sci.* **2012**, *5*, 6460.
(10) Wang, C.-L.; Chang, Y.-C.; Lan, C.-M.; Lo, C.-F.; Diau, E. W.; Lin, C.-Y. *Energy Environ. Sci.* **2011**, *4*, 1788.
(11) Wu, C.-H.; Pan, T.-Y.; Hong, S.-H.; Wang, C.-L.; Kuo, H.-H.; Chu, Y.-Y.; Diau, E. W.-G.; Lin, C.-Y. *Chem. Commun.* **2012**, *48*, 4329.
(12) Li, L.-L.; Diau, E. W.-G. *Chem. Soc. Rev.* **2013**, *42*, 291.
(13) Campbell, W. M.; Jolley, K. W.; Wagner, P.; Wagner, K.; Walsh, P. J.; Gordon, K. C.; Schmidt-Mende, L.; Nazeeruddin, M. K.; Wang, Q.; Grätzel, M.; Officer, D. L. *J. Phys. Chem. C* **2007**, *111*, 11760.
(14) Chang, Y. C.; Wang, C. L.; Pan, T. Y.; Hong, S. H.; Lan, C. M.; Kuo, H. H.; Lo, C. F.; Hsu, H. Y.; Lin, C. Y.; Diau, E. W. *Chem. Commun. (Cambridge, U. K.)* **2011**, *47*, 8910.
(15) Wang, C.-L.; Lan, C.-M.; Hong, S.-H.; Wang, Y.-F.; Pan, T.-Y.; Chang, C.-W.; Kuo, H.-H.; Kuo, M.-Y.; Diau, E. W.-G.; Lin, C.-Y. *Energy Environ. Sci.* **2012**, *5*, 6933.
(16) Yella, A.; Lee, H.-W.; Tsao, H. N.; Yi, C.; Chandiran, A. K.; Nazeeruddin, M. K.; Diau, E. W.-G.; Yeh, C.-Y.; Zakeeruddin, S. M.; Grätzel, M. *Science* **2011**, *334*, 629.
(17) Luo, J.; Xu, M.; Li, R.; Huang, K.-W.; Jiang, C.; Qi, Q.; Zeng, W.; Zhang, J.; Chi, C.; Wang, P.; Wu, J. *J. Am. Chem. Soc.* **2013**, *136*, 265.
(18) Wang, C.-L.; Hu, J.-Y.; Wu, C.-H.; Kuo, H.-H.; Chang, Y.-C.; Lan, Z.-J.; Wu, H.-P.; Wei-Guang Diau, E.; Lin, C.-Y. *Energy Environ. Sci.* **2014**, *7*, 1392.
(19) Kurotobi, K.; Toude, Y.; Kawamoto, K.; Fujimori, Y.; Ito, S.; Chabera, P.; Sundström, V.; Imahori, H. *Chem.—Eur. J.* **2013**, *19*, 17075.
(20) Park, J. K.; Chen, J.; Lee, H. R.; Park, S. W.; Shinokubo, H.; Osuka, A.; Kim, D. *J. Phys. Chem. C* **2009**, *113*, 21956.
(21) Lin, V.; DiMagno, S.; Therien, M. *Science* **1994**, *264*, 1105.
(22) Angiolillo, P. J.; Lin, V. S. Y.; Vanderkooi, J. M.; Therien, M. J. *J. Am. Chem. Soc.* **1995**, *117*, 12514.
(23) Dy, J. T.; Tamaki, K.; Sanehira, Y.; Nakazaki, J.; Uchida, S.; Kubo, T.; Segawa, H. *Electrochemistry* **2009**, *77*, 206.
(24) Yella, A.; Mai, C.-L.; Zakeeruddin, S. M.; Chang, S.-N.; Hsieh, C.-H.; Yeh, C.-Y.; Grätzel, M. *Angew. Chem., Int. Ed.* **2014**.
(25) Mathew, S.; Yella, A.; Gao, P.; Humphry-Baker, R.; CurchodBasile, F. E.; Ashari-Astani, N.; Tavernelli, I.; Rothlisberger, U.; Nazeeruddin, M. K.; Grätzel, M. *Nat. Chem.* **2014**, *6*, 242.
(26) Lee, C.-H.; Galoppini, E. *J. Org. Chem.* **2010**, *75*, 3692.
(27) Rochford, J.; Chu, D.; Hagfeldt, A.; Galoppini, E. *J. Am. Chem. Soc.* **2007**, *129*, 4655.
(28) Ooyama, Y.; Inoue, S.; Nagano, T.; Kushimoto, K.; Ohshita, J.; Imae, I.; Komaguchi, K.; Harima, Y. *Angew. Chem., Int. Ed.* **2011**, *50*, 7429.

(29) Ooyama, Y.; Nagano, T.; Inoue, S.; Imae, I.; Komaguchi, K.; Ohshita, J.; Harima, Y. *Chem.—Eur. J.* **2011**, *17*, 14837.
(30) Lu, J.; Xu, X.; Li, Z.; Cao, K.; Cui, J.; Zhang, Y.; Shen, Y.; Li, Y.; Zhu, J.; Dai, S.; Chen, W.; Cheng, Y.; Wang, M. *Chem.—Asian J.* **2013**, *8*, 956.
(31) Daphnomili, D.; Landrou, G.; Prakash Singh, S.; Thomas, A.; Yesudas, K.; K, B.; Sharma, G. D.; Coutsolelos, A. G. *RSC Adv.* **2012**, *2*, 12899.
(32) Adler, A. D.; Longo, F. R.; Finarelli, J. D.; Goldmacher, J.; Assour, J.; Korsakoff, L. *J. Org. Chem.* **1967**, *32*, 476.
(33) Boutagy, J.; Thomas, R. *Chem. Rev.* **1974**, *74*, 87.
(34) Collman, J. P.; Gagne, R. R.; Halbert, T. R.; Marchon, J. C.; Reed, C. A. *J. Am. Chem. Soc.* **1973**, *95*, 7868.
(35) Hayashi, T.; Miyahara, T.; Hashizume, N.; Ogoshi, H. *J. Am. Chem. Soc.* **1993**, *115*, 2049.
(36) Setsune, J.-i.; Hashimoto, M.; Shiozawa, K.; Hayakawa, J.-y.; Ochi, T.; Masuda, R. *Tetrahedron* **1998**, *54*, 1407.
(37) Satake, A.; Kobuke, Y. *Tetrahedron* **2005**, *61*, 13.
(38) Gouterman, M. *J. Mol. Spectrosc.* **1961**, *6*, 138.
(39) Barea, E. M.; Caballero, R.; Fabregat-Santiago, F.; De La Cruz, P.; Langa, F.; Bisquert, J. *ChemPhysChem* **2010**, *11*, 245.
(40) Clarke, T. M.; Durrant, J. R. *Chem. Rev.* **2010**, *110*, 6736.
(41) Liang, M.; Chen, J. *Chem. Soc. Rev.* **2013**, *42*, 3453.
(42) Kung, H. H.; Jarrett, H. S.; Sleight, A. W.; Ferretti, A. *J. Appl. Phys.* **1977**, *48*, 2463.
(43) Santos, T. D.; Morandeira, A.; Koops, S.; Mozer, A. J.; Tsekouras, G.; Dong, Y.; Wagner, P.; Wallace, G.; Earles, J. C.; Gordon, K. C.; Officer, D.; Durrant, J. R. *J. Phys. Chem. C* **2010**, *114*, 3276.
(44) Usami, A.; Seki, S.; Mita, Y.; Kobayashi, H.; Miyashiro, H.; Terada, N. *Sol. Energy Mater. Sol. Cells* **2009**, *93*, 840.
(45) Marinado, T.; Nonomura, K.; Nissfolk, J.; Karlsson, M. K.; Hagberg, D. P.; Sun, L.; Mori, S.; Hagfeldt, A. *Langmuir* **2009**, *26*, 2592.
(46) Bisquert, J.; Vikhrenko, V. S. *J. Phys. Chem. B* **2004**, *108*, 2313.
(47) Bisquert, J.; Fabregat-Santiago, F.; Mora-Seró, I.; Garcia-Belmonte, G.; Giménez, S. *J. Phys. Chem. C* **2009**, *113*, 17278.
(48) Peter, L. M. *J. Phys. Chem. C* **2007**, *111*, 6601.
(49) Zervaki, G. E.; Roy, M. S.; Panda, M. K.; Angaridis, P. A.; Chrissos, E.; Sharma, G. D.; Coutsolelos, A. G. *Inorg. Chem.* **2013**, *52*, 9813.
(50) Zervaki, G. E.; Papastamatakis, E.; Angaridis, P. A.; Nikolaou, V.; Singh, M.; Kurchania, R.; Kitsopoulos, T. N.; Sharma, G. D.; Coutsolelos, A. G. *Eur. J. Inorg. Chem.* **2014**, *2014*, 1020.
(51) Zervaki, G. E.; Angaridis, P. A.; Koukaras, E. N.; Sharma, G. D.; Coutsolelos, A. G. *Inorg. Chem. Front.* **2014**, *1*, 256.
(52) Sharma, G. D.; Zervaki, G. E.; Angaridis, P. A.; Vatikioti, A.; Gupta, K. S. V.; Gayathri, T.; Nagarjuna, P.; Singh, S. P.; Chandrasekharam, M.; Banthiya, A.; Bhanuprakash, K.; Petrou, A.; Coutsolelos, A. G. *Org. Electron.* **2014**, *15*, 1324.
(53) Work in progress.